Results in Physics 12 (2019) 996–1001

Contents lists available at ScienceDirect

Results in Physics

journal homepage: www.elsevier.com/locate/rinp

# Topological insulator properties of photonic kagome helical waveguide arrays

Hua Zhong[a,b,c], Rong Wang[a,b,c], Fangwei Ye[d], Jingwen Zhang[b,c], Lei Zhang[b,c], Yanpeng Zhang[b,c], Milivoj R. Belić[e], Yiqi Zhang[a,b,c,*]

[a] Guangdong Xi'an Jiaotong University Academy, Foshan 528300, China
[b] Key Laboratory for Physical Electronics and Devices of the Ministry of Education & Shaanxi Key Lab of Information Photonic Technique, Xi'an Jiaotong University, Xi'an 710049, China
[c] School of Electronic and Information Engineering, Xi'an Jiaotong University, Xi'an, Shaanxi 710049, China
[d] School of Physics and Astronomy, Shanghai Jiao Tong University, Shanghai 200240, China
[e] Science Program, Texas A&M University at Qatar, P.O. Box 23874 Doha, Qatar

ARTICLE INFO

*Keywords:*
Kagome lattice
Topological insulator
Edge state

ABSTRACT

We investigate topological insulator properties of the kagome helical waveguide array, by utilizing theoretical and numerical means. The time-reversal symmetry of the kagome lattice is broken by helicity, and a photonic topological insulator is formed. The Berry curvature and Chern number of the band structure are calculated, to verify the topological phase transition, caused by the helicity. Unidirectional propagation and topological protection properties of the edge states at certain momentum values are demonstrated. Interestingly, the same kagome helical waveguide array, may support topological edge states with different momenta propagating along the same boundary but in opposite directions.

## 1. Introduction

Topological insulators (TIs) are electronic materials with a bulk band gap and protected conducting states on their edges or surfaces. They display topological edge states in the band gap which separate energy bands with different topological invariants. By breaking the time-reversal symmetry, the topological protection arises and the edge states can propagate unidirectionally along the edges of a TI without backscattering, even in the presence of defects and disorders [1,2]. Originating from the condensed matter physics, the concept of TIs has speedily percolated to other areas of physics, such as acoustics [3,4], mechanics [5], physics of cold atoms [6–9], photonics [10–20], and others. Different from the condensed matter physics, where it is connected with the electronic transport on the surface, the topological phase transition in photonic crystals cannot be observed by applying magnetic field or by using magnetic materials [21], since the magnetic effects at optical frequencies are much weaker than the electric effects. As a result, to investigate topological effects in photonic systems, which are connected with the transport of photons, alternative mechanisms have to be invented. Until now, novel photonic topological properties have been reported in gyromagnetic photonic crystals [10,11], semiconductor quantum wells [12], arrays of coupled resonators [22,23], metamaterial superlattices [13], and polaritons in microcavities [24–26]. It is worth mentioning that designs based on helical waveguide arrays [16,27–31] and the valley Hall effect [32,33], which do not rely on magnetic field, are becoming popular in the research of topological edge states.

Thus far, there have been several types of lattices [34–44] employed in investigating photonic topological properties, among which the honeycomb lattice [34–36] and Lieb lattices [37–39] were most frequently utilized. On the other hand, the related kagome lattice was not investigated in-depth and as thoroughly as the above-mentioned lattices [45,46,42,43,47–52,44], especially in optics and photonics.

As it is well known, the kagome lattice, a popular Japanese basket pattern, has three sites in the unit cell that form an equilateral triangle—so it is not a Bravais lattice. In addition, the kagome lattice can be understood as a honeycomb lattice with the centers of the triangles located at the lattice points [53,54]. According to the nearest-neighbor tight-binding approximation, the kagome lattice possesses one flat band that is similar to the Lieb lattice and six Dirac cones between the other two bands that are similar to the honeycomb lattice. As a result, the kagome lattice is an excellent candidate for investigating the topological properties of underlying materials. From this point of view, we will investigate the photonic topological properties of kagome lattice by

* Corresponding author at: Xi'an Jiaotong University, Xi'an, Shaanxi 710049, China.
*E-mail address:* zhangyiqi@mail.xjtu.edu.cn (Y. Zhang).

https://doi.org/10.1016/j.rinp.2018.12.053
Received 26 November 2018; Received in revised form 11 December 2018; Accepted 11 December 2018
Available online 25 December 2018

utilizing a helical waveguide array as an example, which can be conveniently produced by employing the femtosecond laser writing technique [55–57]. Even though the honeycomb and Lieb helical waveguide arrays have been reported in [16,58], the kagome helical waveguide array is still worth discussing, since it is not a simple duplication of honeycomb and Lieb lattices. We believe that a well organized research on kagome lattice may bring potential applications in photonics, in producing optical delay lines [22] and lasing systems [59,60].

The organization of this article is as follows. In Section 2, we introduce the theoretical model, and display the band structure as well as the corresponding Berry curvatures of each band. In Section 3, we investigate the band structure of strained kagome lattices, with different boundaries. In Section 4, the propagation of the topological edge states is discussed in details. The robustness of such arrangements is also discussed. In addition, we present topological edge states that may propagate along opposite directions in this waveguide array. We conclude the paper with a short summary in Section 5.

## 2. Band structure and Berry curvatures

The paraxial wave equation that describes the propagation of light in the system is a Schrödinger-like equation of the form

$$i\frac{\partial\psi(x,y,z)}{\partial z} = -\frac{1}{2k_0}\nabla^2\psi(x,y,z) - k_0\frac{\Delta n(x,y,z)}{n_0}\psi(x,y,z), \tag{1}$$

where $\psi(x,y,z)$ is the envelope of the light beam, $k_0 = 2\pi n_0/\lambda$ is the wavenumber in the medium, $\lambda$ is the wavelength, $n_0$ is the background refractive index, and $\Delta n(x,y,z)$ is the refractive index change. Here, $z$ is the propagation direction that plays the role of time, and $x$, $y$ are the transverse coordinates. Similar to the previous research [16,34], the medium adopted here is fused silica, so that $n_0 = 1.45$. Other parameters used in this paper are similar to those in Refs. [16,33] (the wavelength $\lambda = 633$ nm, the longitudinal period $Z = 1$ cm, the distance between two nearest sites $a = 15$ μm, the refractive index change $\Delta n = 1\times10^{-3}$) except for some that needed to be specified.

For the purpose of producing time-symmetry breaking in the system, we transform Eq. (1) into the rotating frame, to obtain a waveguide array in a helical form along the $z$ axis. This is accomplished through the coordinate transformation: $x' = x + R\cos(\Omega z)$, $y' = y + R\sin(\Omega z)$ and $z' = z$, with $R$ and $\Omega$ being the radius and the frequency of the helical waveguide array. As a result, Eq. (1) is recast as

$$i\frac{\partial\psi(x',y',z')}{\partial z'} = -\frac{1}{2k_0}[\nabla + i\mathbf{A}(z')]^2\psi(x',y',z') - k_0\frac{R^2\Omega^2}{2}\psi(x',y',z') - k_0\frac{\Delta n(x',y')}{n_0}\psi(x',y',z'), \tag{2}$$

where $\mathbf{A}(z') = k_0R\Omega[\sin(\Omega z'), -\cos(\Omega z')]$ is equivalent to a vector potential introduced by the helical transformation. Based on Eq. (2) and according to the tight-binding approximation, one obtains the following coupled mode equations [61]:

$$\begin{aligned}
i\tfrac{\partial\psi_{1,m,n}(z')}{\partial z'} =& t[\tau_{12}^*(\mathbf{e}_2)\psi_{2,m+1,n+1}(z') + \tau_{12}(\mathbf{e}_2)\psi_{2,m-1,n-1}(z')] + \\
& t[\tau_{13}^*(\mathbf{e}_3)\psi_{3,m-1,n+1}(z') + \tau_{13}(\mathbf{e}_3)\psi_{3,m+1,n-1}(z')], \\
i\tfrac{\partial\psi_{2,m,n}(z')}{\partial z'} =& t[\tau_{21}^*(\mathbf{e}_2)\psi_{1,m+1,n+1}(z') + \tau_{21}(\mathbf{e}_2)\psi_{1,m-1,n-1}(z')] + \\
& t[\tau_{23}(\mathbf{e}_1)\psi_{3,m,n+2}(z') + \tau_{23}^*(\mathbf{e}_1)\psi_{3,m,n-2}(z')], \\
i\tfrac{\partial\psi_{3,m,n}(z')}{\partial z'} =& t[\tau_{31}^*(\mathbf{e}_3)\psi_{1,m-1,n+1}(z') + \tau_{31}(\mathbf{e}_3)\psi_{1,m+1,n-1}(z')] + \\
& t[\tau_{32}(\mathbf{e}_1)\psi_{2,m,n+2}(z') + \tau_{32}^*(\mathbf{e}_1)\psi_{2,m,n-2}(z')],
\end{aligned} \tag{3}$$

where $t$ is the coupling coefficient, $(m, n)$ are the integers that enumerate the lattice sites, $\psi_{1,2,3}(z')$ represent the wavefunctions at the three sites in one unit cell, and $\mathbf{e}_{1,2,3}$ are the unit vectors of the cell. The details are indicated in Fig. 1(a). In Eq. (3), the asterisk represents the conjugation operation and $\tau_{mn} = \exp[i\mathbf{A}(z')\cdot\mathbf{r}_{mn}]$ are introduced according to the Peierls substitution [16], in which $\mathbf{r}_{mn} = \mathbf{e}_{1,2,3}$ with three possible subindices are determined according to Eq. (3).

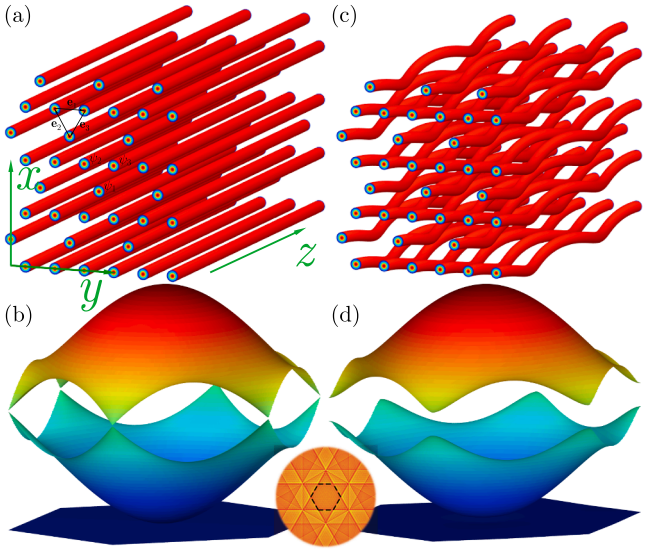


**Fig. 1.** (a) Straight kagome waveguide array. (b) Band structure corresponding to (a). (c) Helical kagome waveguide array. (d) Band structure corresponding to (b). Inset shows the Brillouin zones of the kagome lattice and the region enclosed by the dashed lines is the first Brillouin zone.

For a straight waveguide array, as shown in Fig. 1(a), $\mathbf{A}(z')$ is always zero, so that $\tau_{mn} = 1$ for all the cases. The corresponding band structure is displayed in Fig. 1(b). As expected, there is one flat band and two bands connected by six Dirac points. When the waveguide array is helical along the $z$ axis, with the radius of the helix $R = 5$ μm, as exhibited in Fig. 1(c), the corresponding band structure is depicted in Fig. 1(d). Clearly, the Dirac points between the upper two bands disappear, the reason being that the vector potential $\mathbf{A}(z')$ breaks the time-reversal symmetry of the system, and the topological phase transition happens. We also find that the flat band becomes a dispersive band, which is different from the Lieb lattice, in which the flat band is preserved even when the waveguide array is helical [58]. This means that the symmetry properties of the Lieb lattice are better preserved than those of the kagome lattice, and the Berry curvature (i.e., the pseudo-magnetic field) of the flat band is not zero any longer. In fact, a kagome lattice can be regarded as a deformed Lieb lattice—the angle between $\psi_2 \leftrightarrow \psi_3$ and $\psi_1 \leftrightarrow \psi_3$ changes from $\pi/2$ to $\pi/3$.

We also display the far-field diffraction pattern of the kagome lattice in the inset of Fig. 1. As indicated by the dashed line, the first Brillouin zone of the kagome lattice is the same as that of the honeycomb lattice.

The Berry curvature of a band is given by

$$\mathscr{F}_n = i\sum_{n'\neq n}\frac{\langle u_n|\partial_{k_x}H(\mathbf{k})|u_{n'}\rangle\langle u_{n'}|\partial_{k_y}H(\mathbf{k})|u_n\rangle - (k_x\leftrightarrow k_y)}{(\beta_n-\beta_n')^2}, \tag{4}$$

where $n$ indicates the band number, $H$ is the Hamiltonian of the system, $|u_n\rangle$ and $\beta_n$ are the quasi-energy eigenstates and eigenvalues of $H$, *i.e.*, $H(\mathbf{k})|u_n(\mathbf{k})\rangle = \beta_n(\mathbf{k})|u_n(\mathbf{k})\rangle$. Based on the Berry curvature, the Chern number (the topological invariant number) can be obtained according to

$$C_n = \frac{1}{2\pi}\int_{\mathrm{BZ}} d\mathbf{k}\mathscr{F}_n(\mathbf{k}), \tag{5}$$

where BZ stands for the first Brillouin zone. Corresponding to the bands in Fig. 1(d), the Berry curvatures in the first Brillouin zone are shown in Fig. 2. In Fig. 2(a), the Berry curvature is completely negative, and the corresponding Chern number is $C_1 = -1$. In Fig. 2(b), the situation becomes a bit more complex. The Berry curvature at the six corners of the first Brillouin zone is positive, however it is negative in the middle of

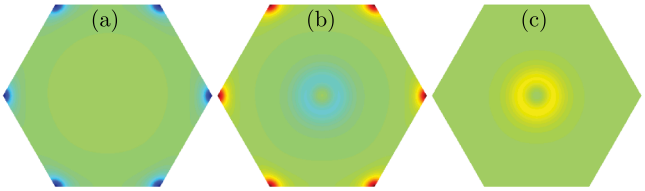


**Fig. 2.** Berry curvatures of the first (top) band (a), second (middle) band (b) and third (bottom) band (c) in Fig. 1(d), respectively. The panels are in the same color scale. Blue means negative, red means positive.

the zone. Calculation demonstrates that $C_2 = 0$ and $\frac{1}{2\pi}\int_{BZ} d\mathbf{k}|\mathscr{F}_2(\mathbf{k})| = 2$; that is, the separate summations of the negative part and positive part give $-1$ and $+1$, respectively. The Berry curvature of the "flat" band is displayed in Fig. 2(c), which is completely positive, and the corresponding Chern number is $C_3 = 1$. According to the bulk-edge correspondence, one can predict the existence of an edge state between the two bands.

## 3. Edge states

Similar to the honeycomb lattice, the strained kagome lattice possesses several different boundaries, and different boundary conditions may lead to different topological edge states.

An interesting case is when the lattice is strained along the $x$ axis but is periodic along the $y$ axis, as shown in Fig. 3(a). In the figure, the left and right boundaries are flat and armchair, respectively, and in the $y$ direction, the boundary type is zigzag. The corresponding band structure is presented in Figs. 3(b) and 3(c). In Fig. 3(b), the straight kagome waveguide array is presented (viz. $R = 0$). The red branches are the non-topological edge states corresponding to the armchair boundary, while the black branches are the bulk modes. One finds that there is no edge state for the flat boundary. We would like to mention that there is flat edge states in a honeycomb lattice waveguide array without helicity [62]. But the edge states are a bit different in the kagome lattice. As shown in Fig. 3(b), the edge states are not flat but dispersive. If the waveguide array is longitudinally helical (along the $z$ direction) with $R = 15\mu$m, the Floquet band structure is shown in Fig. 3(c). As it can be observed, the edge states have become asymmetric about $k_y = 0.5K$, where $K = \pi/a$ is the width of the first Brillouin zone. Unlike the edge state in Fig. 3(b), the edge state here is non-trivial topological and topologically protected.

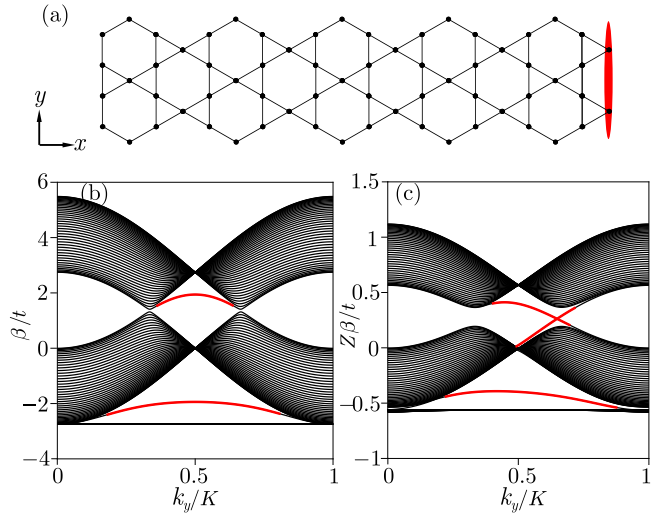


**Fig. 3.** (a) Kagome lattice strained along $x$ axis with armchair and flat boundaries. (b) The static band structure, with $R = 0$. (c) Band structure with $R = 15\,\mu$m. The edge states are shown in red, which are located at the edge indicated by the red ellipse in (a).

Taking the edge state at $k_y = 0.5K$ as an example, the group velocity of the state $d\beta/dk_y$ is zero in Fig. 3(b) but nonzero in Fig. 3(c). The edge state in Fig. 3(b) is perfectly symmetric, while in Fig. 3(c) it is not. Note that the edge state is not so obvious for the flat boundary in Fig. 3(c), but numerical simulations demonstrate that such an edge state will emerge with increasing helical radius $R$ and the asymmetry of the edge state of the armchair boundary will become more apparent. In the band gap between the first two bands, the two kinds of edge states from different boundaries cross around the valley. Very recently, we became aware of similar results displayed in Ref. [63]. Since the larger the value of $R$, the more severe bending loss, we do not consider anymore the edge state corresponding to the flat boundary in this paper.

## 4. Transport properties

Now, we discuss the propagation of edge states, to examine the topological transport properties. We construct a kagome lattice waveguide array with armchair boundaries by superposing Gaussian functions in the index change,

$$\Delta n(x, y, z) = \sum_{m,n} p\exp\left(-\frac{[x + R\cos(\Omega z) - x_{m,n}]^2 + [y + R\sin(\Omega z) - y_{m,n}]^2}{w^2}\right), \tag{6}$$

with $p = 1 \times 10^{-3}$, $w = 0.5a$, and with $(x_{m,n}, y_{m,n})$ denoting the location of the specific waveguide. The input facet of the waveguide array is shown in Fig. 4(a).

### 4.1. Straight waveguide array

To start with, we consider the straight case of $R = 0$. In order to excite the edge state, we launch an elongated Gaussian beam $\psi(x, y, z = 0) = \exp[(x - x_0)^2/w_1^2 + y^2/w_2^2]\exp(ik_y y)$ into the left armchair boundary of kagome lattice, as presented in Fig. 4(b1). In the Gaussian beam, $w_1 = 0.5a\,(w_2 = 10a)$ indicate the widths of the beam along $x\,(y)$ axis, and $x_0$ is the location of the left boundary of the

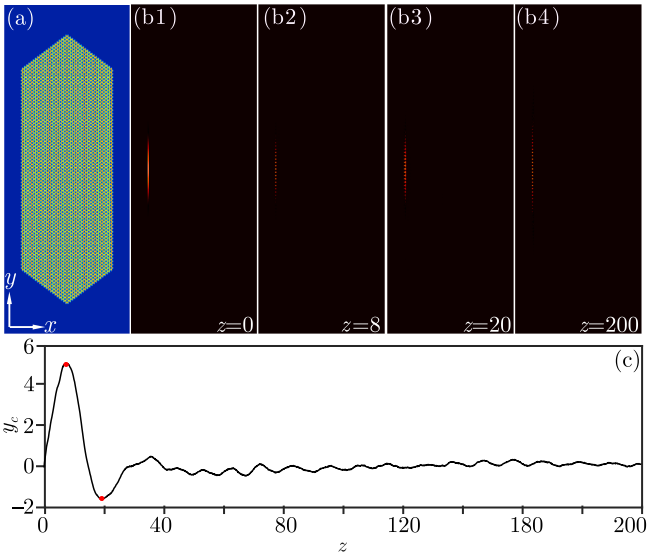


**Fig. 4.** (a) Input facet of the waveguide array, showing armchair boundaries. (b1)–(b4) Edge state intensity distributions at chosen propagation distances. The input beam is launched into the left boundary of the lattice, as shown in (b1). The domain shown in (a) and (b1–b4) is $x \in [-50a, 50a]$ and $y \in [-100a, 100a]$. (c) Center of mass of the edge state along $y$ axis during propagation. The two red dots correspond to (b2) and (b3), respectively.

waveguide array. Figs. 4(b2)-4(b4) depict the intensity distributions of the beam at certain distances. Naturally, when propagating in a waveguide array, the continuous beam breaks into beamlets in different waveguides. In a normal linear propagation, owing to the coupling between waveguides, the beam tends to spread. However, here during propagation, the beam that excites the edge state stays at the same position on the left armchair boundary and does not develop the horizontal or vertical displacement. To see the localization more clearly, we describe the vertical center of mass of the beam via

$$y_c(z) = \frac{\iint y|\psi(x, y, z)|^2 dxdy}{\iint |\psi(x, y, z)|^2 dxdy}, \tag{7}$$

and the result is shown in Fig. 4(c). One can see that except for the beam balancing adjustment to reach a steady state at the beginning, during the whole propagation, the beam center just oscillates with a small fluctuation around $y = 0$. The reason for this phenomenon is quite natural—the group velocity of the non-helical edge state at $k_y = 0.5K$ is zero.

### 4.2. Helical waveguide array

To confirm the robustness and immunity to backscattering of topologically protected edge states, we consider the longitudinal helical waveguide array with the radius $R = 5\mu$m. Since the group velocity of edge states is nonzero, the beam that excites the edge state will no longer remain at the same position, but propagate along the edge in the prescribed direction. Utilizing the same input beam as in Fig. 4(b), the corresponding propagation dynamics is displayed in Fig. 5 at chosen propagation distances. The propagation is also indicated in the Movie 1. One finds that the beam indeed propagates along the armchair boundary unidirectionally without experiencing significant backscattering, even when rounding the corners.

### 4.3. The influence of defects

Next, we introduce a defect into the kagome lattice waveguide array, to display the robust resistance of the topological edge states to the appearance of defects. The defect is realized by removing one waveguide on the left boundary, and the corresponding lattice geometry is shown in Fig. 6(a). Launching the same input Gaussian beam into the left boundary of the lattice waveguide array with a defect, the propagation is displayed in Figs. 6(b)–(e) at the chosen distances. Obviously, the topologically protected edge state passes through the defect smoothly. We present the complete propagation in Movie 2. It should be mentioned that the input Gaussian beam inevitably excites some bulk states, and this is the reason why there is some reflected energy, which is completely scattered ultimately during propagation.

These phenomena indicate that by introducing the longitudinal helical modulation into the kagome lattice waveguide array, the time-reversal symmetry of the system is broken, and one obtains

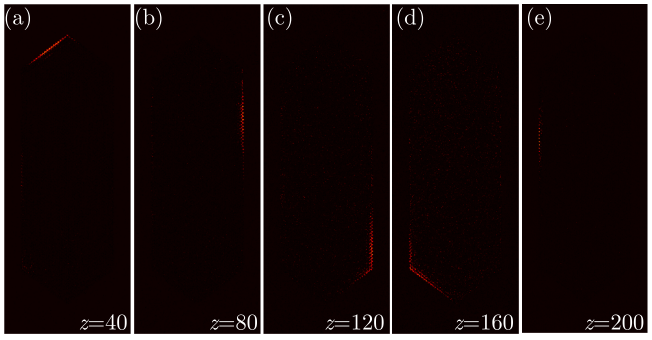


**Fig. 5.** Propagation of the topological edge state at different propagation distances [Movie 1]. Parameters: $R = 5$ μm and $k_y = 0.5$ K.

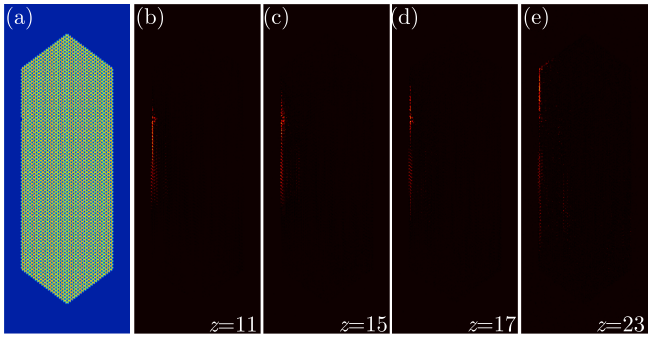


**Fig. 6.** (a) Input face geometry of the kagome helical waveguide arrays with a defect barrier. (b)–(e) The intensity distribution at the different propagation distances [Movie 2].

topologically protected edge states which can propagate unidirectionally and are shielded from the backscattering, even when encountering a defect. Nonetheless, note that we do not talk here about the large helical rotation radius in the longitudinal direction, because then the bending losses become large, which leads to a leakage of optical power into the bulk that affect the topologically protected properties of edge states [16].

### 4.4. Edge states with opposite propagating directions

Finally, we consider the edge states with opposite propagating directions in the same lattice. According to the band structure in Fig. 3, the edge state of the kagome lattice is non-monotonous (i.e., the sign of $d\beta/dk$ is different at different $k$), which is different from the case of the honeycomb lattice. This difference means that the launched beams carrying different momenta may excite the edge states with opposite propagating directions (even in the straight waveguide array), which presents therefore an advantage of the kagome lattice. Practically, this can be easily achieved through adjusting the incident angle of the launched beam [34].

To display this advantage, we choose $k_y = 0.27$ K in the launched Gaussian beam and do propagation in the same setup as that of Fig. 5. Some typical intensity distributions at certain distances are displayed in Fig. 7. Different from the case with $k_y = 0.5$ K (Figs. 5 and 6) that propagates clockwise, the beam here propagates anti-clockwise. Therefore, one can obtain topological edge states with opposite propagating directions even in the sample with the same boundaries.

We would like to note that edge states with opposite propagating directions are still topologically protected, and this is not contradictory to the unidirectional propagating property of the edge state. The launched beam that excites the edge state at different $k$ may propagate unidirectionally in opposite directions, still with topological protection.

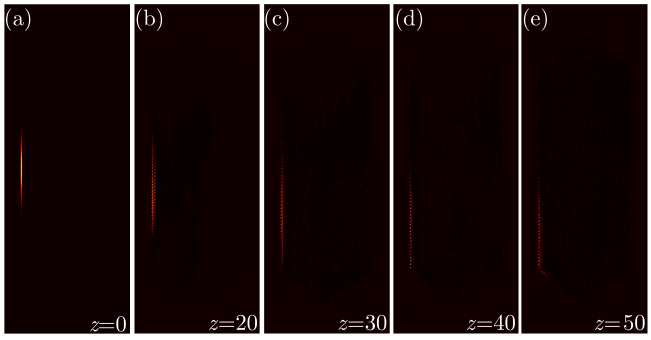


**Fig. 7.** Counter-propagating edge state. Setup is as Fig. 5, but with $k_y = 0.27$ K.

## 5. Conclusion

We have presented the topological insulator properties of edge states in the kagome lattice by introducing the longitudinal helical modulation, to break the time-reversal symmetry of the system. Due to helicity, the Dirac points as well as the flat band in the band structure disappear. Berry curvature and the corresponding Chern number of each band are calculated, and we find that the Chern numbers of the first, second and third band are − 1, 0, and 1, respectively. The unidirectional propagation and the topological protection properties (immunity to defects) of the topological edge states are demonstrated through constructing a photonical kagome lattice potential, encircled by the armchair boundaries. Last but not least, we find that topological edge states with different momenta can propagate in opposite directions, and are topologically protected in the same sample of the kagome lattice, along the same boundary. Our research indicates that kagome lattices can serve as good platforms for investigating photonic topological insulators, and the results may lead to potential applications in producing on-chip functional optical devices, such as optical switches and isolators, to name a few.

## Acknowledgments

The work was supported by Natural Science Foundation of Guangdong Province (2018A0303130057) and Shaanxi Province (2017JZ019), and Qatar National Research Fund (NPRP 8-028-1-001). MRB acknowledges support by the Al Sraiya Holding Group.

## Appendix A. Supplementary data

Supplementary data associated with this article can be found, in the online version, athttps://doi.org/10.1016/j.rinp.2018.12.053.

## References

[1] Hasan MZ, Kane CL. Colloquium: topological insulators. Rev Mod Phys 2010;82:3045–67. https://doi.org/10.1103/RevModPhys. 82.3045.
[2] Qi X-L, Zhang S-C. Topological insulators and superconductors. Rev Mod Phys 2011;83:1057–110. https://doi.org/10.1103/RevModPhys.83.1057.
[3] Yang Z, Gao F, Shi X, Lin X, Gao Z, Chong Y, et al. Topological acoustics. Phys Rev Lett 2015;114:114301. https://doi.org/10.1103/PhysRevLett. 114.114301.
[4] He C, Ni X, Ge H, Sun X-C, Chen Y-B, Lu M-H, et al. Acoustic topological insulator and robust one-way sound transport. Nat Phys 2016;12:1124–9. https://doi.org/10.1038/nphys3867.
[5] Huber SD. Topological mechanics. Nat Phys 2016;12:621–3. https://doi.org/10.1038/nphys3801.
[6] Jotzu G, Messer M, Desbuquois R, Lebrat M, Uehlinger T, Greif D, et al. Experimental realisation of the topological Haldane model. Nature 2014;515:237–40. https://doi.org/10.1038/nature13915.
[7] Leder M, Grossert C, Sitta L, Genske M, Rosch A, Weitz M. Real-space imaging of a topologically protected edge state with ultracold atoms in an amplitude-chirped optical lattice. Nat Commun 2016;7:13112. https://doi.org/10.1038/ncomms13112.
[8] Beeler MC, Williams RA, Jiménez-García K, LeBlanc LJ, Perry AR, Spielman IB. The spin Hall effect in a quantum gas. Nature 2013;498:201–4. https://doi.org/10.1038/nature12185.
[9] Kennedy CJ, Siviloglou GA, Miyake H, Burton WC, Ketterle W. Spin-orbit coupling and quantum spin hall effect for neutral atoms without spin flips. Phys Rev Lett 2013;111:225301. https://doi.org/10.1103/PhysRevLett. 111.225301.
[10] Haldane FDM, Raghu S. Possible realization of directional optical waveguides in photonic crystals with broken time-reversal symmetry. Phys Rev Lett 2008;100:013904. https://doi.org/10.1103/PhysRevLett. 100.013904.
[11] Wang Z, Chong Y, Joannopoulos JD, Soljacic M. Observation of unidirectional backscattering-immune topological electromagnetic states. Nature 2009;461:772–5. https://doi.org/10.1038/nature08293.
[12] Lindner NH, Refael G, Galitski V. Floquet topological insulator in semiconductor quantum wells. Nat Phys 2011;7(6):490–5. https://doi.org/10.1038/nphys1926.
[13] Khanikaev AB, Mousavi SH, Tse W-K, Kargarian M, MacDonald AH, Shvets G. Photonic topological insulators. Nat Mater 2012;12:233–9. https://doi.org/10.1038/nmat3520.
[14] Chen W-J, Jiang S-J, Chen X-D, Zhu B, Zhou L, Dong J-W, et al. Experimental realization of photonic topological insulator in a uniaxial metacrystal waveguide. Nat Commun 2014;5:5782. https://doi.org/10.1038/ncomms6782.
[15] Dong J-W, Chen X-D, Zhu H, Wang Y, Zhang X. Valley photonic crystals for control of spin and?topology. Nat Mater 2016;16:298–302. https://doi.org/10.1038/nmat4807.
[16] Rechtsman MC, Zeuner JM, Plotnik Y, Lumer Y, Podolsky D, Dreisow F, et al. Photonic Floquet topological insulators. Nature 2013;496:196–200. https://doi.org/10.1038/nature12066.
[17] Maczewsky LJ, Zeuner JM, Nolte S, Szameit A. Observation of photonic anomalous Floquet topological insulators. Nat Commun 2017;8:13756. https://doi.org/10.1038/ncomms13756.
[18] Mukherjee S, Spracklen A, Valiente M, Andersson E, Öhberg P, Goldman N, et al. Experimental observation of anomalous topological edge modes in a slowly driven photonic lattice. Nat Commun 2017;8:13918. https://doi.org/10.1038/ncomms13918.
[19] Bandres MA, Rechtsman MC, Segev M. Topological photonic quasicrystals: fractal topological spectrum and protected transport. Phys Rev X 2016;6:011016. https://doi.org/10.1103/PhysRevX.6.011016.
[20] Weimann S, Kremer M, Plotnik Y, Lumer Y, Nolte S, Makris KG, et al. Topologically protected bound states in photonic parity-time-symmetric crystals. Nat Mater 2016;16:433–8. https://doi.org/10.1038/nmat4811.
[21] Chang C-Z, Zhang J, Feng X, Shen J, Zhang Z, Guo M, et al. Experimental observation of the quantum anomalous Hall effect in a magnetic topological insulator. Science 2013;340(6123):167–70. https://doi.org/10.1126/science.1234414. arXiv: http://science.sciencemag.org/content/340/6129/167.full.pdf.
[22] Hafezi M, Demler EA, Lukin MD, Taylor JM. Robust optical delay lines with topological protection. Nat Phys 2011;7:907–12. https://doi.org/10.1038/nphys2063.
[23] Umucalílar RO, Carusotto I. Fractional quantum Hall states of photons in an array of dissipative coupled cavities. Phys Rev Lett 2012;108:206809. https://doi.org/10.1103/PhysRevLett. 108.206809.
[24] Nalitov AV, Solnyshkov DD, Malpuech G. Polariton Z topological insulator. Phys Rev Lett 2015;114:116401. https://doi.org/10.1103/PhysRevLett. 114.116401.
[25] Kartashov YV, Skryabin DV. Modulational instability and solitary waves in polariton topological insulators. Optica 2016;3(11):1228–36. https://doi.org/10.1364/OPTICA.3.001228. URLhttp://www.osapublishing.org/optica/abstract.cfm?URI=optica-3-11-1228.
[26] Kartashov YV, Skryabin DV. Bistable topological insulator with exciton-polaritons. Phys Rev Lett 2017;119:253904. https://doi.org/10.1103/PhysRevLett. 119.253904.
[27] Rechtsman MC, Plotnik Y, Zeuner JM, Song D, Chen Z, Szameit A, et al. Topological creation and destruction of edge states in photonic graphene. Phys Rev Lett 2013;111:103901. https://doi.org/10.1103/PhysRevLett. 111.103901.
[28] Ablowitz MJ, Curtis CW, Ma Y-P. Linear and nonlinear traveling edge waves in optical honeycomb lattices. Phys Rev A 2014;90:023813. https://doi.org/10.1103/PhysRevA.90.023813.
[29] Ablowitz MJ, Ma Y-P. Strong transmission and reflection of edge modes in bounded photonic graphene. Opt Lett 2015;40(20):4635–8. https://doi.org/10.1364/OL.40.004635. URLhttp://ol.osa.org/abstract.cfm?URI=ol-40-20-4635.
[30] Leykam D, Rechtsman MC, Chong YD. Anomalous topological phases and unpaired dirac cones in photonic Floquet topological insulators. Phys Rev Lett 2016;117:013902. https://doi.org/10.1103/PhysRevLett. 117.013902.
[31] Zhang W, Zhang X, Kartashov YV, Chen X, Ye F. Bloch oscillations in arrays of helical waveguides. Phys Rev A 2018;97:063845. https://doi.org/10.1103/PhysRevA.97.063845.
[32] Wu X, Meng Y, Tian J, Huang Y, Xiang H, Han D, et al. Direct observation of valley-polarized topological edge states in designer surface plasmon crystals. Nat Commun 2017;8(1):1304. https://doi.org/10.1038/s41467-017-01515-2.
[33] Noh J, Huang S, Chen KP, Rechtsman MC. Observation of photonic topological valley Hall edge states. Phys Rev Lett 2018;120:063902. https://doi.org/10.1103/PhysRevLett. 120.063902.
[34] Plotnik Y, Rechtsman MC, Song D, Heinrich M, Zeuner JM, Nolte S, et al. Observation of unconventional edge states in 'photonic graphene'. Nat Mater 2014;13:57–62. https://doi.org/10.1038/nmat3783.
[35] Song D, Paltoglou V, Liu S, Zhu Y, Gallardo D, Tang L, et al. Unveiling pseudospin and angular momentum in photonic graphene. Nat Commun 2015;6:6272.
[36] Zhang YQ, Wu ZK, Belić MR, Zheng HB, Wang ZG, Xiao M, et al. Photonic Floquet topological insulators in atomic ensembles. Laser Photon Rev 2015;9:331–8.
[37] Vicencio RA, Cantillano C, Morales-Inostroza L, Real B, Mejía-Cortés C, Weimann S, et al. Observation of localized states in Lieb photonic lattices. Phys Rev Lett 2015;114:245503. https://doi.org/10.1103/PhysRevLett. 114.245503.
[38] Mukherjee S, Spracklen A, Choudhury D, Goldman N, Öhberg P, Andersson E, et al. Observation of a localized flat-band state in a photonic Lieb lattice. Phys Rev Lett 2015;114:245504. https://doi.org/10.1103/PhysRevLett. 114.245504.
[39] Diebel F, Leykam D, Kroesen S, Denz C, Desyatnikov AS. Conical diffraction and composite Lieb bosons in photonic lattices. Phys Rev Lett 2016;116:183902. https://doi.org/10.1103/PhysRevLett. 116.183902.
[40] Lan Z, Goldman N, Öhberg P. Coexistence of spin-$\frac{1}{2}$ and spin-1 Dirac-Weyl fermions in the edge-centered honeycomb lattice. Phys Rev B 2012;85:155451. https://doi.org/10.1103/PhysRevB.85.155451.
[41] Zhong H, Zhang YQ, Zhu Y, Zhang D, Li CB, Zhang YP, et al. Transport properties in the photonic super-honeycomb lattice – a hybrid fermionic and bosonic system. Ann Phys (Berlin) 2017;529(3):1600258. https://doi.org/10.1002/andp.201600258.
[42] Guo H-M, Franz M. Topological insulator on the kagome lattice. Phys Rev B 2009;80:113102. https://doi.org/10.1103/PhysRevB.80.113102.
[43] Liu G, Zhu S-L, Jiang S, Sun F, Liu WM. Simulating and detecting the quantum spin Hall effect in the kagome optical lattice. Phys Rev A 2010;82:053605. https://doi.org/10.1103/PhysRevA.82.053605.
[44] Gulevich DR, Yudin D, Skryabin DV, Iorsh IV, Shelykh IA. Exploring nonlinear topological states of matter with exciton-polaritons: edge solitons in kagome lattice. Sci Rep 2017;7(1):1780. https://doi.org/10.1038/s41598-017-01646-y.

[45] Ohgushi K, Murakami S, Nagaosa N. Spin anisotropy and quantum Hall effect in the kagomé lattice: chiral spin state based on a ferromagnet. Phys Rev B 2000;62:R6065–8. https://doi.org/10.1103/PhysRevB.62.R6065.
[46] Atwood JL. Kagomé lattice: a molecular toolkit for magnetism. Nat Mater 2002;1:91–2. https://doi.org/10.1038/nmat740.
[47] Boguslawski M, Rose P, Denz C. Nondiffracting kagome lattice. Appl Phys Lett 2011;98:061111. https://doi.org/10.1063/1.3554759. URLhttp://scitation.aip.org/content/aip/journal/apl/98/6/10.1063/1.3554759.
[48] Jo G-B, Guzman J, Thomas CK, Hosur P, Vishwanath A, Stamper-Kurn DM. Ultracold atoms in a tunable optical kagome lattice. Phys Rev Lett 2012;108:045305. https://doi.org/10.1103/PhysRevLett. 108.045305.
[49] Nakata Y, Okada T, Nakanishi T, Kitano M. Observation of flat band for terahertz spoof plasmons in a metallic kagomé lattice. Phys Rev B 2012;85:205128. https://doi.org/10.1103/PhysRevB.85.205128.
[50] Liu R, Chen W-C, Wang Y-F, Gong C-D. Topological quantum phase transitions and topological flat bands on the kagomé lattice. J Phys: Condens Matter 2012;24(30):305602.
[51] He C, Zhang Z. Floquet topological phase transitions and chiral edge states in a kagome lattice. Phys Lett A 2014;378(43):3200–4. https://doi.org/10.1016/j.physleta.2014.09.029. URLhttp://www.sciencedirect.com/science/article/pii/S037596011400930X.
[52] Zong Y, Xia S, Tang L, Song D, Hu Y, Pei Y, et al. Observation of localized flat-band states in kagome photonic lattices. Opt Express 2016;24:8877–85. https://doi.org/10.1364/OE.24.008877. URLhttp://www.opticsexpress.org/abstract.cfm?URI=oe-24-8-8877.
[53] Björkman T, Skakalova V, Kurasch S, Kaiser U, Meyer JC, Smet JH, Krasheninnikov AV. Vibrational properties of a two-dimensional silica kagome lattice. ACS Nano 2016;10(12):10929–35. https://doi.org/10.1021/acsnano.6b05577. pMID: 28024359. arXiv: https://doi.org/10.1021/acsnano.6b05577.
[54] Björkman T, Kurasch S, Lehtinen O, Kotakoski J, Yazyev OV, Srivastava A, et al. Defects in bilayer silica and graphene: common trends in diverse hexagonal two-dimensional systems. Sci Rep 2013;3:3482. https://doi.org/10.1038/srep03482.
[55] Davis KM, Miura K, Sugimoto N, Hirao K. Writing waveguides in glass with a femtosecond laser. Opt Lett 1996;21:1729–31. https://doi.org/10.1364/OL.21.001729. URLhttp://ol.osa.org/abstract.cfm?URI=ol-21-21-1729.
[56] Szameit A, Nolte S. Discrete optics in femtosecond-laser-written photonic structures. J Phys B: At Mol Opt Phys 2010;43:163001. URLhttp://stacks.iop.org/0953-4075/43/i=16/a=163001.
[57] Tang H, Lin X-F, Feng Z, Chen J-Y, Gao J, Sun K. Experimental two-dimensional quantum walk on a photonic chip. Sci Adv 2018;4(5):eaat3174. https://doi.org/10.1126/sciadv.aat3174. arXiv: http://advances.sciencemag.org/content/4/5/eaat3174.full.pdf,http://advances.sciencemag.org/content/4/5/eaat3174.
[58] Bandres MA, Rechtsman M, Szameit A, Segev M. Lieb photonic topological insulator. In: CLEO: 2014, Optical Society of America; 2014. p. FF2D.3. doi: https://doi.org/10.1364/CLEO_QELS.2014.FF2D.3.http://www.osapublishing.org/abstract.cfm?URI=CLEO_QELS-2014-FF2D.3.
[59] Harari G, Bandres MA, Lumer Y, Rechtsman MC, Chong YD, Khajavikhan M, et al. Topological insulator laser Theory. Science 2018;359(6381). https://doi.org/10.1126/science.aar4003. eaar4003.arXiv: http://science.sciencemag.org/content/359/6381/eaar4003.full.pdf.
[60] Bandres MA, Wittek S, Harari G, Parto M, Ren J, Segev M, Christodoulides DN, et al. Topological insulator laser: experiments. Science 2018;359(6381):eaar4005. https://doi.org/10.1126/science.aar4005. arXiv: http://science.sciencemag.org/content/359/6381/eaar4005.full.pdf, URLhttp://science.sciencemag.org/content/359/6381/eaar4005.
[61] Szameit A, Rechtsman MC, Bahat-Treidel O, Segev M. $\mathscr{PT}$-symmetry in honeycomb photonic lattices. Phys Rev A 2011;84:021806. https://doi.org/10.1103/PhysRevA.84.021806.
[62] Fujita M, Wakabayashi K, Nakada K, Kusakabe K. Peculiar localized state at zigzag graphite edge. J Phys Soc Jap 1996;65(7):1920–3. https://doi.org/10.1143/JPSJ.65.1920.
[63] Ablowitz MJ, Cole JT. Tight-binding equations for longitudinally driven waveguides: Lieb and kagome lattices, arXiv preprint; 2018. 1804.09880.